

Granular Ta-Te nanowire superconductivity violating the Pauli limit

Lingxiao Zhao^{1#}, Yi Zhao^{1#}, Cuiying Pei¹, Changhua Li¹, Qi Wang^{1,2}, Juefei Wu¹,
Weizheng Cao¹, Lin Xiong^{1,3}, Haiyin Zhu^{1,3}, Tianping Ying⁴, Yanpeng Qi^{1,2,3*}

1. School of Physical Science and Technology, ShanghaiTech University, 201210 Shanghai, China.
2. ShanghaiTech Laboratory for Topological Physics, ShanghaiTech University, 201210 Shanghai, China
3. Shanghai Key Laboratory of High-resolution Electron Microscopy, ShanghaiTech University, 201210 Shanghai, China
4. Institute of Physics and University of Chinese Academy of Sciences, Chinese Academy of Sciences, 100190 Beijing, China

These authors contributed to this work equally.

* Correspondence should be addressed to Y.Q. (qiyp@shanghaitech.edu.cn)

Abstract: Strategies to achieve higher upper-critical-field superconductors ($\mu_0 H_{c2}(0)$) are of great interest for both fundamental science and practical applications. While reducing the thickness of two-dimensional (2D) materials to a few layers significantly enhances $\mu_0 H_{c2}(0)$ with accompanied potential unconventional pairing mechanisms, further dimensional reduction to 1D compounds rarely exceeds the expected Pauli limit. Here, we report the discovery of a 1D granular Ta-Te nanowire that becomes superconducting under high pressure, with a maximum critical temperature (T_c) of 5.1 K. Remarkably, the $\mu_0 H_{c2}(0)$ reaches 16 T, which is twice the Pauli limit, setting a record of $\mu_0 H_{c2}(0)$ in all the reported 1D superconductors. Our work demonstrates that the Ta-Te nanowire not only is a potential candidate for applications in high magnetic fields, but also provides an ideal platform for further investigations of the mechanisms between nanowires and large $\mu_0 H_{c2}(0)$.

Introduction

Since the discovery of the Meissner effect, efforts for pursuing superconductors with higher upper critical fields ($\mu_0 H_{c2}(0)$) have never been paused. In recent years, the success in mechanical exfoliation of 2D van der Waals materials has unveiled many new superconductors with large upper critical fields, especially in nano-films of transition metal chalcogenides (TMCs). Few-layer NbSe₂ is reported to be an Ising superconductor and exhibits orbital Fulde-Ferrell-Larkin-Ovchinnikov (FFLO) states

under large magnetic fields¹⁻⁵. As a result, the in-plane $\mu_0 H_{c2}(0)$ of few-layer NbSe₂ is about 1.5 times of Pauli limit ($\mu_0 H_p$). Similar behaviors are also observed in MoS₂⁶, TaS₂⁷ and gated WS₂⁸.

The discovery of large upper critical fields in 2D materials inspires the exploration of further reducing their dimensions, which may lead to higher $\mu_0 H_p$ and possibly unconventional superconductivity. However, reports of superconductivity in 1D nanowires violating the Pauli limit are extremely rare. To the best of our knowledge, Bi nanowires are reported to show complex superconducting properties, depending on the morphology of the nanowires⁹⁻¹¹. Single crystal Bi nanowires' T_c and $\mu_0 H_{c2}(0)$ are 1.3 K and 4 T, respectively¹⁰. In contrast, granular nanowires of Bi exhibit 8.3 K and 4.5 T, which show similar behavior to the bulk high-pressure phase, Bi-V⁹. Another example is the B nanowire, which is insulating at ambient pressure, but superconducting at 84 GPa. The $\mu_0 H_{c2}(0)$ of B nanowires is about 2.5 T while the T_c is only about 1.5 K¹². In the cases of single crystal Bi nanowires and pressurized B nanowires, the upper critical fields are quite large considering their low T_c . Apart from high pressure, proximity effects and ion beams can also induce superconductivity in nanowires¹³⁻¹⁵. Therefore, the dependences of the critical behavior of superconducting nanowires on morphology, pressure, gating, proximity effect, and synthesis methods are quite complex, little consensus has been reached up to now.

In this work, we synthesized a novel TMC nanowire composed of Ta₃Te₄ granules. The nanowires show semi-metal behavior at ambient pressure and superconductivity under high pressure. The upper critical field reaches about 16 T at 21 GPa, which is about 4 times T_c and much larger than the value of Pauli limit. The $\mu_0 H_{c2}(0) - T_c$ ratio is the highest among all the reported superconducting nanowires. We have successfully combined the advantages of TMC compounds, nanowires and high-pressure modulations, realizing a large upper critical field in compressed Ta-Te nanowires.

Ta-Te nanowires are synthesized by the chemical vapor transport (CVT) method¹⁶. A Stoichiometric amount of 99.999% tantalum and tellurium powder (Alfar Aesar) is mixed and sealed in evacuated silica ampoules. The starting powder in each ampoule weighs 1 gram and 20 mg of iodine as the transport agent. The size of the ampoules used is 10 cm (length) * 1.5 cm (diameter). The sealed ampoules are heated to 1100 °C in 10 hours, and annealed for 24 hours in a box furnace. The small temperature gradient in the box furnace is enough for the growth of the nanowires. The nanowires are black, and show fiber-like texture, with typical dimensions of 100 nm * 100 nm * 100 μm. They are densely tangled, forming bundles, as shown in Figure S1.

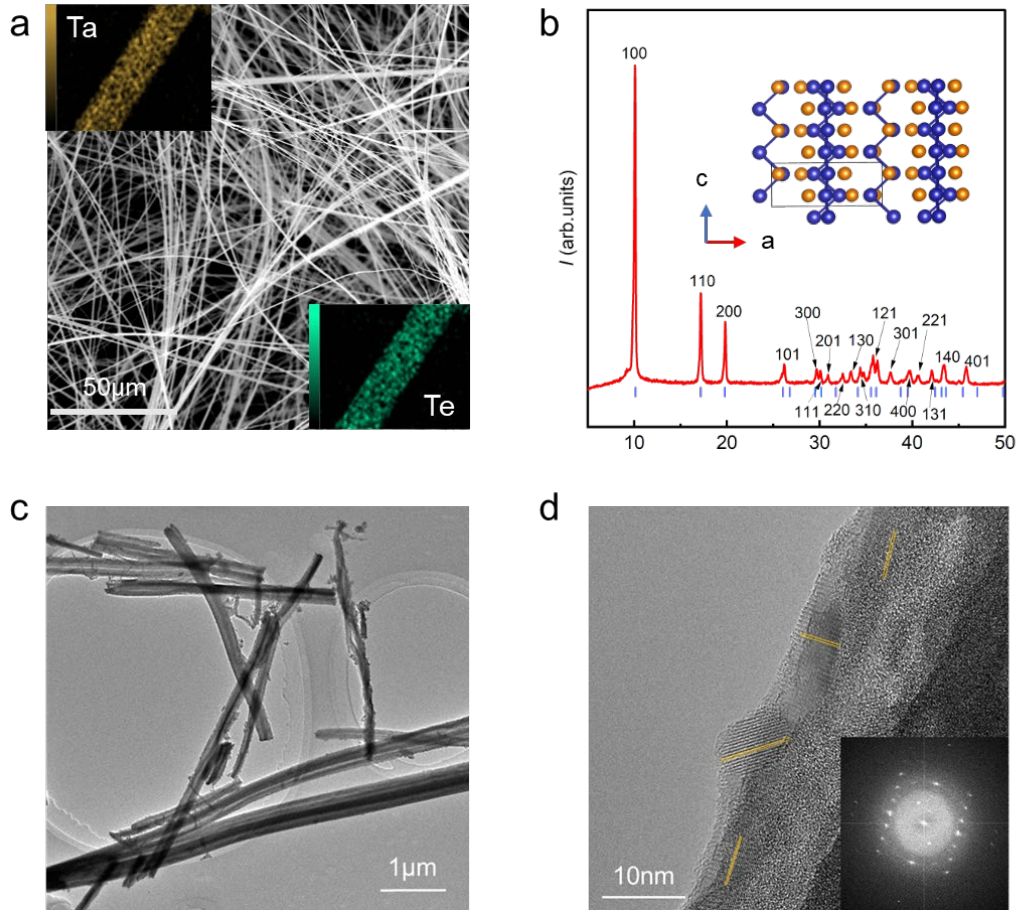


Figure 1. Structural characterization of Ta-Te nanowires at ambient pressure. (a) The SEM image of the nanowires under low magnification. The insets show elemental mapping under SEM. (b) Powder XRD results of a bunch of nanowires. The inset shows the crystal structure of Ta-Te nanowires. (c) The TEM image of the nanowires under low magnification. (d) The TEM images of a nanowire under high magnification. The inset shows the fast Fourier transform (FFT) of the images.

A low magnification SEM image of the synthesized samples is presented in Figure 1a. Under higher magnification, we performed elemental dispersion spectrum (EDS) mapping of a single nanowire. The results are exhibited in the insets of Figure 1a. We observe that Ta and Te atoms are uniformly distributed in the nanowire. We have also conducted powder X-ray diffraction (XRD) measurements on a bunch of nanowires directly acquired from synthesis, as shown in Figure 1b. Though the strongly anisotropic orientation of the nanowires causes difficulty in Rietveld refinements, we have confirmed that the indexed XRD peaks are correlated to the hexagonal Nb₃Te₄ structure¹⁷, with the space group P6₃/m, as shown in the inset of Figure 1b. It is worth noting that the average full width at half maximum of the diffraction peaks is 0.2°. Using the Scherrer equation, the estimated grain size is 58 nm, implying that these 1D samples may be composed of numerous small nanocrystals.

To further investigate the appearance and morphology of the nanowires, we have performed high magnification SEM and TEM observations. From Figure 1a, we can observe that the nanowires directly collected from synthesis are densely tangled. The samples we used for the following high-pressure *in-situ* resistivity measurements are of the same appearance as the bundle of nanowires near the right edge of Figure S1. The nearly isolated nanowire in the middle of Figure S1 is used for resistivity measurements at ambient pressure.

The samples for TEM are prepared by dispersion of nanowires into ethanol using ultrasonic methods. The dispersed nanowires are transferred to copper grids with carbon membranes. As shown in the low magnification image in Figure 1d, the dispersed samples stand on the carbon membranes. Some of the nanowires are slightly distorted or twisted due to local stress.

High-resolution TEM image of a single nanowire is shown in Figure 1d. The nanowires are composed of crystalline granules. The orientations of the crystalline granules are slightly random, as indicated by yellow lines in Figure 1d. The insets show the fast fourier transformations (FFT) of the images. In the FFT results, "amorphous" halos are observed. This indicates that the grain boundaries exhibit disordered structure. The nanowires thus have bamboo-like structures.

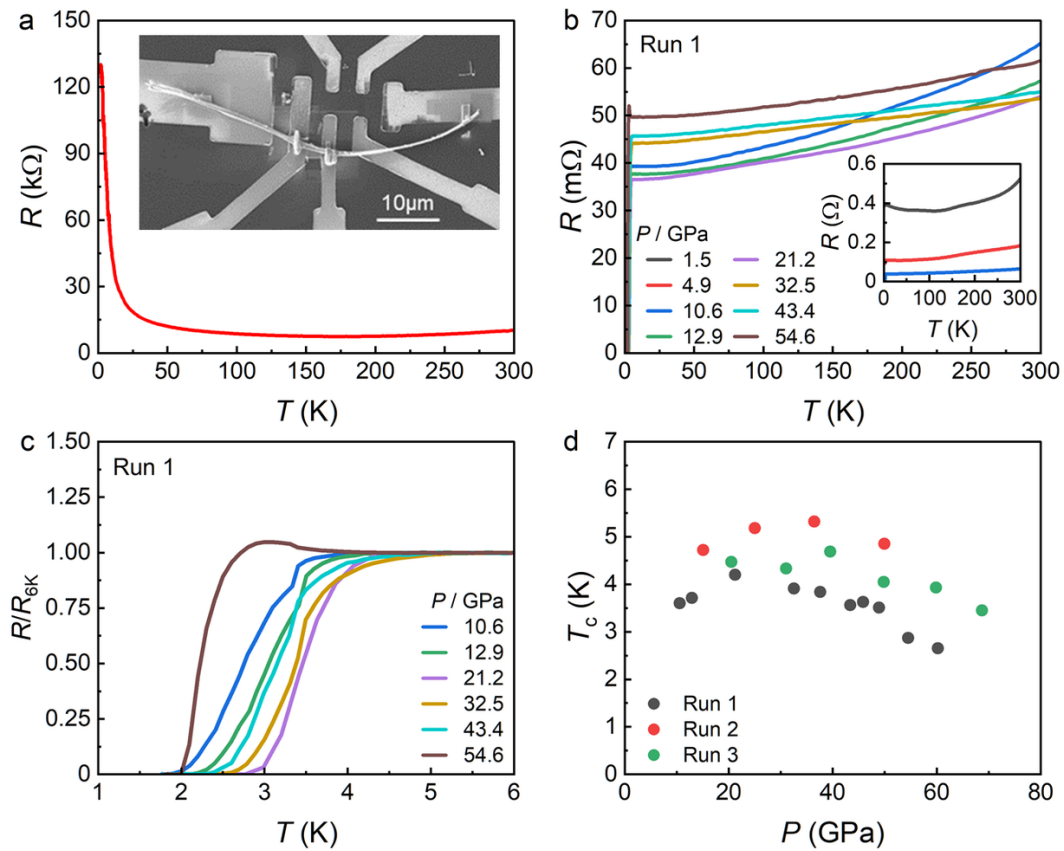


Figure 2. Resistivity measurements of Ta-Te nanowires. (a) The temperature dependence of resistivity at ambient pressure. The inset shows the setup of electrodes

and focused ion beam (FIB) transported sample. (b) The temperature dependence of resistivity under 1.5-54.6 GPa. (c) The normalized temperature dependence of resistivity at low temperature. (d) The T_c -Pressure phase diagram.

The temperature dependence of resistivity of a single nanowire at ambient pressure is summarized in Figure 2a. The sample is transported to pre-set electrodes by focused ion beam (FIB) under SEM (Inset of Figure 1e). We use ionic deposited Pt to contact the sample with the electrodes. The nanowire shows an insulator-type electronic transport property, as shown in Figure 2a. The resistivity first slightly drops with cooling temperature. At about 200 K, it turns to increase rapidly, showing insulating behavior. This result is quite different from the metallic behavior of its isomer Nb_3Te_4 ¹⁸.

The electronic structure of the sample is quite important, given that the nanowires show semi-metal type transport properties. We have performed IR transmission spectrum on Ta-Te nanowires to deduce the band gap, shown in Figure S2. The transmission rate of IR light with wavelengths from 2 to 15 μm is lower than 1%. So, the optical band gap is at least lower than 75 meV. We suggest that the insulating behavior of the nanowire below 200 K is not a result of the electronic band structure.

Since the samples are insulating at ambient pressure, we attempted utilizing high-pressure to induce superconductivity in Ta-Te nanowires. We have measured the temperature dependence of resistivity from 1.8 K to 300 K under high pressure, as shown in Figure 2b-c. Bunches of tangled nanowires are directly loaded into the sample chamber. At 1.5 GPa, the sample shows insulating behavior, similar to ambient state. It transforms into bad-metal type at 4.9 GPa. During compression, the resistivity at room temperature gradually decreases. At 10.6 GPa, superconductivity onsets at about 3.5 K. The ΔT_c is rather wide at this pressure point, with the resistivity dropping to zero at 2 K. With further compression, T_c shows a dome-like evolution with a maximum of 4.13 K at 21.2 GPa, and it drops slowly to about 2.7 K at the highest-pressure point measured in this work. Other runs of measurements have acquired similar evolutions, as shown in Figure S3-4. The phase diagram of T_c and pressure from multiple runs are summarized in Figure 2d.

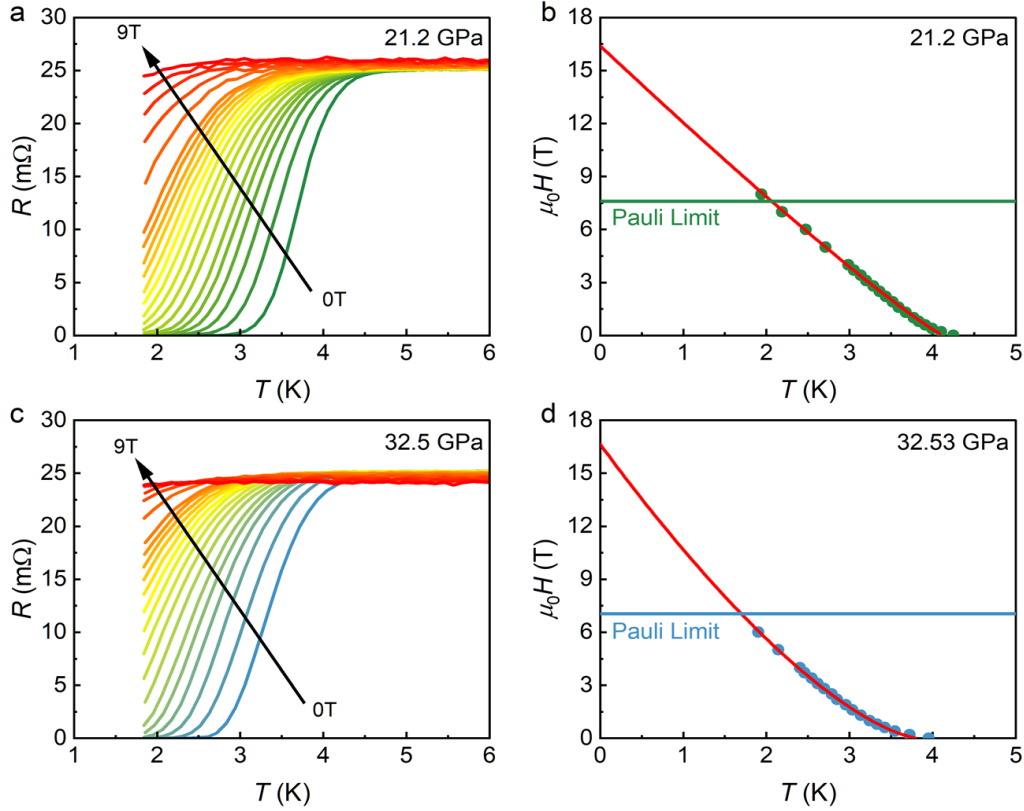


Figure 3. The upper critical field of Ta-Te nanowires. (a) The temperature dependence of resistivity under different magnetic fields from 0 T to 9 T, at 21.2 GPa. (b) The fitted curve of $\mu_0 H_{c2}(T)$ with multi-band model at 21.2 GPa. (c) and (d) are similar to (a) and (b), but at 32.5 GPa. The green line in (b) and blue line in (d) denotes the Pauli limit.

To further investigate the superconductivity properties of Ta-Te nanowires, we have measured the upper critical field of the sample at 21.2 GPa and 32.5 GPa (Figure 3). In Figure 3a and c, as the magnetic field increases, T_c gradually decreases until it disappears above the lowest measured temperature. By defining the temperature where the resistance drops by 90% under the magnetic field as T_c , we plot the $\mu_0 H_{c2}$ against T_c in Figure 3b and d. We then fit the data using the multi-band model. We have found that at 21.2 GPa and 32.53 GPa, the $\mu_0 H_{c2}(0)$ are 16.39 T and 16.64 T, respectively. It should be noted that the Pauli limit $\mu_0 H_p$ at these two pressure points are 7.60 T and 7.05 T, respectively. The $\mu_0 H_{c2}(0)$ results are much higher than $\mu_0 H_p$, exhibiting exotic superconducting behavior.

The Pauli limit violating behavior indicates that the pressure-induced superconductivity in Ta-Te nanowires possibly originates from a complex mechanism. According to literature, the $\mu_0 H_{c2}(0)$ of most superconducting nanowires are near or below the Pauli limit, regardless of the T_c (Figure 4). Compared with them, Ta-Te nanowires show significantly larger $\mu_0 H_{c2}(0)$. In the case of Ta-Te nanowires, the $\mu_0 H_{c2}(0)$ is larger than two times $\mu_0 H_p$. Some 2D TMCs present similar phenomena. For example, few-layer NbSe₂ is an Ising superconductor, with large in-plane $\mu_0 H_{c2}(0)$. It

also turns into FFLO state at low temperature and high magnetic field⁵, with an abrupt upturn of $\mu_0 H_{c2}$ after the transition point in the phase diagram. The large upper critical field of the Ta-Te nanowires may originate from a similar mechanism, since the compositional element Ta is moderately heavy, with strong spin-orbital coupling. However, no signals of upturning FFLO states are observed under 9 T in this work (Figure 3b and d). Large upper critical fields have also been observed in some other unconventional superconductors such as cuprates, iron arsenides, heavy-fermion superconductors, etc¹⁹⁻²⁹. The exotic pairing mechanisms play important roles in enhancing $\mu_0 H_{c2}(0)$. In short, further investigations on the Ta-Te nanowires are required to unveil the pairing mechanism and its influence on the large $\mu_0 H_{c2}(0)$. Apart from the pairing mechanisms of large $\mu_0 H_{c2}(0)$ observed in these materials, there might be exotic unknown origin in the 1D nanowires. In addition, due to the large upper critical field (16 T) and the moderate T_c (4 K) among known superconducting nanowires, application potentials of Ta-Te nanowires can be expected, considering that the nanowires are easy to synthesize, and may exhibit excellent mechanical properties.

In summary, we propose a granular strategy for Ta-Te nanowires that successfully realizes superconductivity under high pressure and achieves a record-high upper critical field. Superconductivity emerges at 10.6 GPa, with a T_c of about 3.5 K. T_c exhibits a slight dome-like behavior during compression. Ta-Te nanowire is a possible candidate for applications in high magnetic field, and provides an ideal platform for investigating the exotic mechanisms of large upper critical fields.

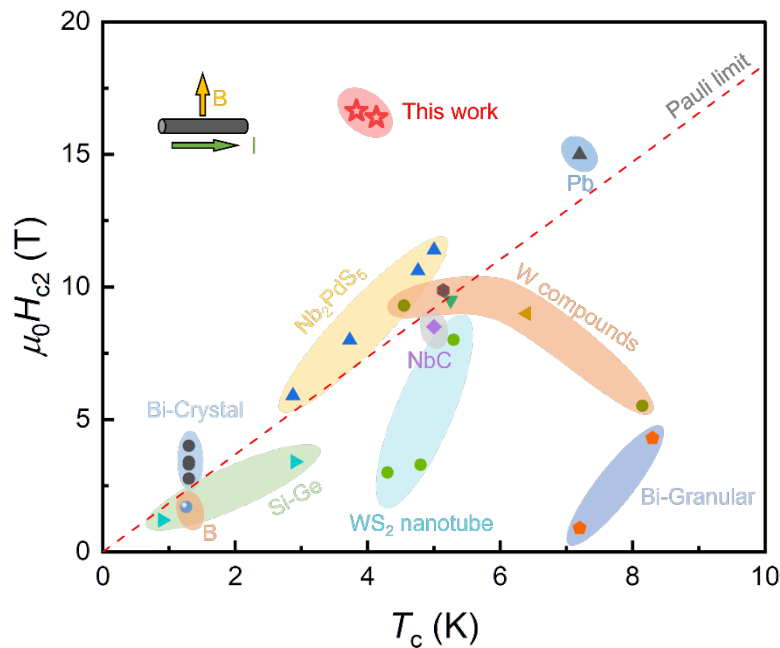


Figure 4. The upper critical fields of several superconducting nanowires. The multiple data points in one type of nanowire represent different diameters. The details are summarized in Table S1.

Supplementary Information

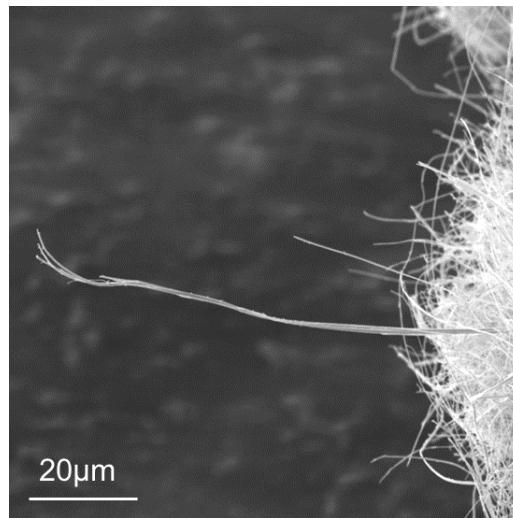


Figure S1. The SEM image of the separated nanowire for ambient resistivity measurements from a bunch of nanowires.

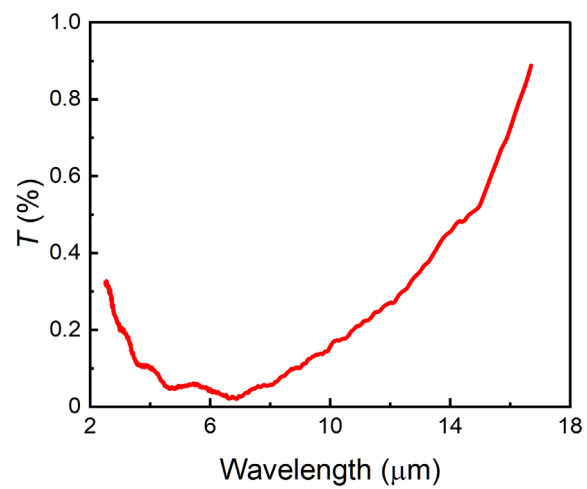


Figure S2. IR transmission spectrum of Ta-Te nanowire.

High-pressure *in-situ* electrical transport property is measured in Physical Property Measurement System (PPMS-9T) using a nonmagnetic diamond anvil cell (DAC). A cubic BN/epoxy mixture is used as insulating layer between BeCu gaskets and electrodes. The nanowires are directly collected from synthesis and then loaded into the diamond anvil cell (DAC) with 200 μm anvil culet. Four Pt foils are arranged in a van der Pauw four-probe configuration to contact the sample in the chamber for resistivity measurements³⁰. Pressure is determined by the ruby luminescence method³¹.

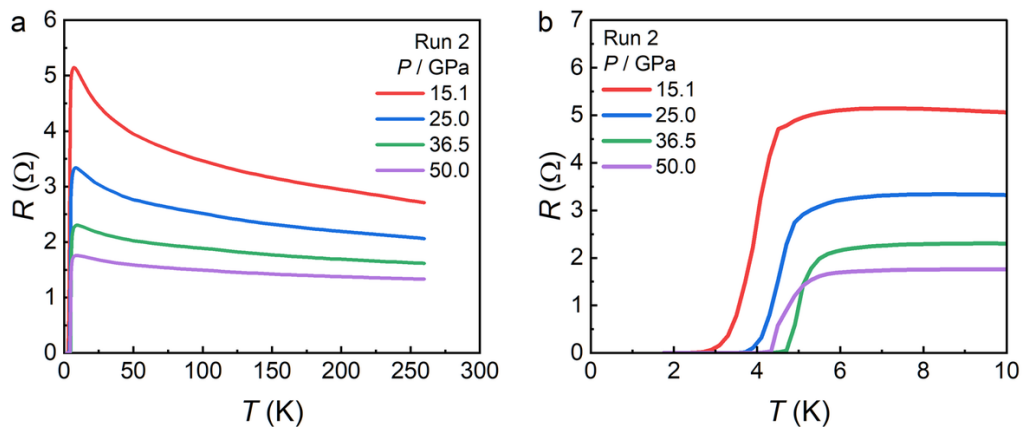


Figure S3. The temperature dependence of resistivity of Ta-Te nanowires under high pressure from Run 2. (a) 1.8 – 265 K. (b) 1.8 – 10 K.

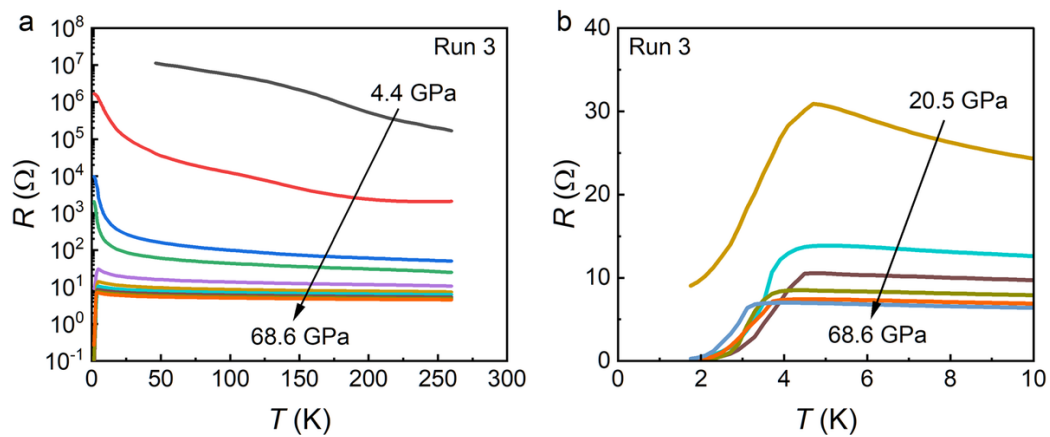


Figure S4. The temperature dependence of resistivity of Ta-Te nanowires under high pressure from Run 3. (a) 1.8 – 265 K. (b) 1.8 – 10 K.

Table S1. The upper critical field in several superconducting nanowires.

Compound	T_c (K)	$\mu_0 H_{c2}(0)$ (T)	$\mu_0 H_{c2}(0) / T_c$	ref
Ta-Te nanowires	3.83	16.64	4.34	This work
Bi	1.3	4	3.07	10
Ta ₂ PdS ₅	5	11.4	2.28	32
Pb	7.2	15	2.08	33
W(CO) ₆	5.25	9.5	1.81	34
NbC	5	8.5	1.7	35
W	4.2	7	1.67	13
He ⁺ Focused WC _{1-x}	6.4	9	1.41	14
B	1.257	1.7	1.35	12
diffused Ge–Si	2.9	3.4	1.17	36
Bi-V	8.3	4.3	0.52	9
Bi-III	7.2	1.0	0.14	9

ACKNOWLEDGMENT

This work was supported by the National Key R&D Program of China (Grant No. 2023YFA1607400) and the National Natural Science Foundation of China (Grant No. 52272265), The authors thank the Analytical Instrumentation Center (# SPST-AIC10112914), SPST, ShanghaiTech University.

REFERENCES

1. Wickramaratne, D.; Khmelevskiy, S.; Agterberg, D. F.; Mazin, I. I., Ising Superconductivity and Magnetism in NbSe₂. *Physical Review X* **2020**, *10* (4), 041003.
2. Zhang, H.; Rousuli, A.; Zhang, K.; Luo, L.; Guo, C.; Cong, X.; Lin, Z.; Bao, C.; Zhang, H.; Xu, S.; Feng, R.; Shen, S.; Zhao, K.; Yao, W.; Wu, Y.; Ji, S.; Chen, X.; Tan, P.; Xue, Q.-K.; Xu, Y.; Duan, W.; Yu, P.; Zhou, S., Tailored Ising superconductivity in intercalated bulk NbSe₂. *Nature Physics* **2022**, *18* (12), 1425-1430.
3. Yi, H.; Hu, L.-H.; Wang, Y.; Xiao, R.; Cai, J.; Hickey, D. R.; Dong, C.; Zhao, Y.-F.; Zhou, L.-J.; Zhang, R.; Richardella, A. R.; Alem, N.; Robinson, J. A.; Chan, M. H. W.; Xu, X.; Samarth, N.; Liu, C.-X.; Chang, C.-Z., Crossover from Ising- to Rashba-type superconductivity in epitaxial Bi₂Se₃/monolayer NbSe₂ heterostructures. *Nature Materials* **2022**, *21* (12), 1366-1372.
4. Li, L.; Zhang, S.; Hu, G.; Guo, L.; Wei, T.; Qin, W.; Xiang, B.; Zeng, C.; Zhang, Z.; Cui, P., Converting a Monolayered NbSe₂ into an Ising Superconductor with Nontrivial Band Topology via Physical or Chemical Pressuring. *Nano Letters* **2022**, *22* (16), 6767-6774.
5. Wan, P.; Zheliuk, O.; Yuan, N. F. Q.; Peng, X.; Zhang, L.; Liang, M.; Zeitler, U.; Wiedmann, S.; Hussey, N. E.; Palstra, T. T. M.; Ye, J., Orbital Fulde–Ferrell–Larkin–Ovchinnikov state in an Ising superconductor. *Nature* **2023**, *619* (7968), 46-51.
6. Lu, J. M.; Zheliuk, O.; Leermakers, I.; Yuan, N. F. Q.; Zeitler, U.; Law, K. T.; Ye, J. T., Evidence for two-dimensional Ising superconductivity in gated MoS₂. *Science* **2015**, *350* (6266), 1353-1357.
7. de la Barrera, S. C.; Sinko, M. R.; Gopalan, D. P.; Sivadas, N.; Seyler, K. L.; Watanabe, K.;

- Taniguchi, T.; Tsen, A. W.; Xu, X.; Xiao, D.; Hunt, B. M., Tuning Ising superconductivity with layer and spin-orbit coupling in two-dimensional transition-metal dichalcogenides. *Nature Communications* **2018**, *9* (1), 1427.
8. Lu, J.; Zheliuk, O.; Chen, Q.; Leermakers, I.; Hussey, N. E.; Zeitler, U.; Ye, J., Full superconducting dome of strong Ising protection in gated monolayer WS₂. *Proceedings of the National Academy of Sciences* **2018**, *115* (14), 3551-3556.
 9. Tian, M.; Wang, J.; Kumar, N.; Han, T.; Kobayashi, Y.; Liu, Y.; Mallouk, T. E.; Chan, M. H. W., Observation of Superconductivity in Granular Bi Nanowires Fabricated by Electrodeposition. *Nano Letters* **2006**, *6* (12), 2773-2780.
 10. Tian, M.; Wang, J.; Ning, W.; Mallouk, T. E.; Chan, M. H. W., Surface Superconductivity in Thin Cylindrical Bi Nanowire. *Nano Letters* **2015**, *15* (3), 1487-1492.
 11. Tian, M.; Wang, J.; Zhang, Q.; Kumar, N.; Mallouk, T. E.; Chan, M. H. W., Superconductivity and Quantum Oscillations in Crystalline Bi Nanowire. *Nano Letters* **2009**, *9* (9), 3196-3202.
 12. Sun, L.; Matsuoka, T.; Tamari, Y.; Shimizu, K.; Tian, J.; Tian, Y.; Zhang, C.; Shen, C.; Yi, W.; Gao, H.; Li, J.; Dong, X.; Zhao, Z., Pressure-induced superconducting state in crystalline boron nanowires. *Physical Review B* **2009**, *79* (14), 140505.
 13. Wang, J.; Shi, C.; Tian, M.; Zhang, Q.; Kumar, N.; Jain, J. K.; Mallouk, T. E.; Chan, M. H. W., Proximity-Induced Superconductivity in Nanowires: Minigap State and Differential Magnetoresistance Oscillations. *Physical Review Letters* **2009**, *102* (24), 247003.
 14. Córdoba, R.; Ibarra, A.; Mailly, D.; De Teresa, J. M., Vertical Growth of Superconducting Crystalline Hollow Nanowires by He⁺ Focused Ion Beam Induced Deposition. *Nano Letters* **2018**, *18* (2), 1379-1386.
 15. Sadki, E. S.; Ooi, S.; Hirata, K., Focused-ion-beam-induced deposition of superconducting nanowires. *Applied Physics Letters* **2004**, *85* (25), 6206-6208.
 16. Edwards, H. K.; Salyer, P. A.; Roe, M. J.; Walker, G. S.; Brown, P. D.; Gregory, D. H., Growth and Microstructural Characterization of Single Crystalline Nb₃Te₄ Nanowires. *Crystal Growth & Design* **2005**, *5* (4), 1633-1637.
 17. Selte, K.; Kjekshus, A., The crystal structures of Nb₃Se₄ and Nb₃Te₄. *Acta Crystallographica* **1964**, *17* (12), 1568-1572.
 18. Ishihara, Y.; Nakada, I., Electrical transport properties of a quasi-one-dimensional Nb₃Te₄ single crystal. *Solid State Communications* **1983**, *45* (2), 129-132.
 19. Cao, Y.; Park, J. M.; Watanabe, K.; Taniguchi, T.; Jarillo-Herrero, P., Pauli-limit violation and re-entrant superconductivity in moiré graphene. *Nature* **2021**, *595* (7868), 526-531.
 20. Chow, L. E.; Yip, K. Y.; Pierre, M.; Zeng, S. W.; Zhang, Z. T.; Heil, T.; Deuschle, J.; Nandi, P.; Sudheesh, S. K.; Lim, Z. S.; Luo, Z. Y.; Nardone, M.; Zitouni, A.; van Aken, P. A.; Goiran, M.; Goh, S. K.; Escoffier, W.; Ariando, A., Pauli-limit violation in lanthanide infinite-layer nickelate superconductors. 2022.
 21. Liu, X.; Zhang, N. J.; Watanabe, K.; Taniguchi, T.; Li, J. I. A., Isospin order in superconducting magic-angle twisted trilayer graphene. *Nature Physics* **2022**, *18* (5), 522-527.
 22. Squire, O. P.; Hodgson, S. A.; Chen, J.; Fedoseev, V.; de Podesta, C. K.; Weinberger, T. I.; Alireza, P. L.; Grosche, F. M., Superconductivity beyond the Conventional Pauli Limit in High-Pressure CeSb_2 . *Physical Review Letters* **2023**, *131* (2), 026001.
 23. Machida, K., Violation of Pauli-Clogston limit in the heavy-fermion superconductor CeRh_2As_2 : Duality of itinerant and localized f electrons. *Physical Review B* **2022**, *106* (18), 184509.
 24. Nakamura, D.; Adachi, T.; Omori, K.; Koike, Y.; Takeyama, S., Pauli-limit upper critical field of high-temperature superconductor La_{1.84}Sr_{0.16}CuO₄. *Scientific Reports* **2019**, *9* (1), 16949.
 25. Gao, Z.; Wang, L.; Qi, Y.; Wang, D.; Zhang, X.; Ma, Y.; Yang, H.; Wen, H., Superconducting properties of granular SmFeAsO_{1-x}F_x wires with T_c = 52 K prepared by the powder-in-tube method. *Superconductor Science and Technology* **2008**, *21* (11), 112001.
 26. Qi, Y.; Gao, Z.; Wang, L.; Wang, D.; Zhang, X.; Ma, Y., Superconductivity at 34.7 K in the iron arsenide Eu_{0.7}Na_{0.3}Fe₂As₂. *New Journal of Physics* **2008**, *10* (12), 123003.
 27. Mercure, J. F.; Bangura, A. F.; Xu, X.; Wakeham, N.; Carrington, A.; Walmsley, P.; Greenblatt, M.; Hussey, N. E., Upper Critical Magnetic Field far above the Paramagnetic Pair-Breaking Limit of Superconducting One-Dimensional $\text{Li}_{0.9}\text{Mo}_6\text{O}_{17}$ Single Crystals. *Physical Review Letters* **2012**, *108* (18), 187003.

28. Lu, J.; Xu, X.; Greenblatt, M.; Jin, R.; Tinnemans, P.; Licciardello, S.; van Delft, M. R.; Buhot, J.; Chudzinski, P.; Hussey, N. E., Emergence of a real-space symmetry axis in the magnetoresistance of the one-dimensional conductor $\text{Li}_{0.9}\text{Mo}_6\text{O}_{17}$. *Science Advances* **2019**, *5* (7), eaar8027.
29. Yang, J.; Luo, J.; Yi, C.; Shi, Y.; Zhou, Y.; Zheng, G.-q., Spin-triplet superconductivity in $\text{K}_2\text{Cr}_3\text{As}_3$. *Science Advances* **2021**, *7* (52), eabl4432.
30. Pei, C.; Zhang, J.; Wang, Q.; Zhao, Y.; Gao, L.; Gong, C.; Tian, S.; Luo, R.; Li, M.; Yang, W.; Lu, Z.-Y.; Lei, H.; Liu, K.; Qi, Y., Pressure-induced superconductivity at 32 K in MoB_2 . *National Science Review* **2023**, *10* (5).
31. Mao, H. K.; Xu, J.; Bell, P. M., Calibration of the ruby pressure gauge to 800 kbar under quasi-hydrostatic conditions. *Journal of Geophysical Research: Solid Earth* **1986**, *91* (B5), 4673-4676.
32. Ning, W.; Yu, H.; Liu, Y.; Han, Y.; Wang, N.; Yang, J.; Du, H.; Zhang, C.; Mao, Z.; Liu, Y.; Tian, M.; Zhang, Y., Superconductor–Insulator Transition in Quasi-One-Dimensional Single-Crystal Nb_2PdS_5 Nanowires. *Nano Letters* **2015**, *15* (2), 869-875.
33. He, M.; Wong, C. H.; Tse, P. L.; Zheng, Y.; Zhang, H.; Lam, F. L. Y.; Sheng, P.; Hu, X.; Lortz, R., “Giant” Enhancement of the Upper Critical Field and Fluctuations above the Bulk T_c in Superconducting Ultrathin Lead Nanowire Arrays. *ACS Nano* **2013**, *7* (5), 4187-4193.
34. Sun, Y.; Wang, J.; Zhao, W.; Tian, M.; Singh, M.; Chan, M. H. W., Voltage-current properties of superconducting amorphous tungsten nanostrips. *Scientific Reports* **2013**, *3* (1), 2307.
35. Porrati, F.; Barth, S.; Sachser, R.; Dobrovolskiy, O. V.; Seybert, A.; Frangakis, A. S.; Huth, M., Crystalline Niobium Carbide Superconducting Nanowires Prepared by Focused Ion Beam Direct Writing. *ACS Nano* **2019**, *13* (6), 6287-6296.
36. Ridderbos, J.; Brauns, M.; de Vries, F. K.; Shen, J.; Li, A.; Kölling, S.; Verheijen, M. A.; Brinkman, A.; van der Wiel, W. G.; Bakkers, E. P. A. M.; Zwanenburg, F. A., Hard Superconducting Gap and Diffusion-Induced Superconductors in Ge–Si Nanowires. *Nano Letters* **2020**, *20* (1), 122-130.